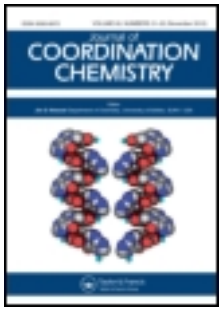


Journal of Coordination Chemistry
Publication details, including instructions for authors and subscription information:
http://www.tandfonline.com/loi/gcoo20

# Syntheses, crystal structures, and magnetism of two phenylacetate imidazolate copper(II) complexes

Hong-Lin Zhu [a], Wei Xu [a], Jian-Li Lin [a], Chun Zhang [a] & Yue-Qing Zheng [a]

[a] Crystal Engineering Division, Center of Applied Solid State Chemistry Research, Ningbo University, Ningbo, 315211 P. R. China

Accepted author version posted online: 17 Sep 2012.Published online: 28 Sep 2012.

To cite this article: Hong-Lin Zhu, Wei Xu, Jian-Li Lin, Chun Zhang & Yue-Qing Zheng (2012) Syntheses, crystal structures, and magnetism of two phenylacetate imidazolate copper(II) complexes, Journal of Coordination Chemistry, 65:22, 3983-3997, DOI: 10.1080/00958972.2012.730145

To link to this article: http://dx.doi.org/10.1080/00958972.2012.730145

*Journal of Coordination Chemistry*
Vol. 65, No. 22, 20 November 2012, 3983–3997



# Syntheses, crystal structures, and magnetism of two phenylacetate imidazolate copper(II) complexes

HONG-LIN ZHU, WEI XU, JIAN-LI LIN, CHUN ZHANG and YUE-QING ZHENG*

Crystal Engineering Division, Center of Applied Solid State Chemistry Research, Ningbo University, Ningbo, 315211 P. R. China

(*Received 20 June 2012; in final form 13 August 2012*)

The influence of pH for the reaction system involving $CuCl_2 \cdot 2H_2O$, imidazole (Him) and phenylacetic acid (HL) at room temperature was investigated. $Cu_2(Him)_4L_4 \cdot 2H_2O$ (**1**) and $Cu_3(Him)_2(im)_2L_4$ (**2**) were synthesized at pH 6.5 and 7.5, respectively. In **1**, the Cu is coordinated by two nitrogen atoms of two Him and three oxygen atoms from three phenylacetates to form a square pyramid $CuN_2O_3$. Adjacent square pyramids share edges to form $Cu_2N_4O_4$ dimers, which are assembled by hydrogen bonds into a 2-D layer parallel to the (001) plane. In **2**, copper atoms are interlinked by $im^-$ and $L^-$ to form a 2-D layer parallel to (100). The resulting layers have C–H···O hydrogen bonds leading to a 3-D supramolecular architecture. Variable temperature magnetism of **1** and **2** suggests a weak ferromagnetic or antiferromagnetic coupling exchange ($J = 0.58\,cm^{-1}$ for **1**, $J = -10.24\,cm^{-1}$ for **2**).

*Keywords*: Supramolecular architecture; Imidazole; Phenylacetic acid; Copper(II); Magnetism



## 1. Introduction

Supramolecular compounds have received attention due to their interesting architectures and properties [1–4]. Supramolecular assemblies can be designed based on non-covalent intermolecular interactions, such as hydrogen bonds, aromatic $\pi\cdots\pi$ stacking interactions, electrostatic and van der Waals forces, and hydrophobic, and hydrophilic interactions. Hydrogen bonding and aromatic $\pi\cdots\pi$ stacking interactions play a fundamental role in supramolecular chemistry [5–7]. The most feasible strategies are choices of coordination geometry of metal ions and polyfunctional ligands that enable the control of structural motifs.

Carboxylic acids have been well documented in the preparation of supramolecular complexes with intermolecular interactions. The carboxylate can be a hydrogen-bond donor or acceptor participating in intermolecular or intramolecular hydrogen bonds to form complexes with different dimensionalities [8–10]. N-donor heteroaromatic ligands such as imidazole are also ideal candidates for the design and synthesis of supramolecular architectures [11–14]. Two types of imidazole ligands exist, neutral

*Corresponding author. Email: yqzhengmc@163.com

*Journal of Coordination Chemistry*
ISSN 0095-8972 print/ISSN 1029-0389 online 
http://dx.doi.org/10.1080/00958972.2012.730145

imidazole molecules (Him) and deprotonated imidazole ($im^-$). The two forms of imidazole provide recognition sites for $\pi$–$\pi$ stacking interactions to form supramolecular structures. Further, Him coordinates with metals monodentate and can also form hydrogen bonds. The $im^-$ usually is bridging and accepts H as a receptor.

To investigate the influence of pH in the reaction of imidazolate, Cu(II), and phenylacetic acid (HL), we herein report two new phenylacetate imidazolate Cu(II) complexes, $Cu_2(Him)_4L_4 \cdot 2H_2O$ (**1**) and $Cu_3(Him)_2(im)_2L_4$ (**2**). Structure determination reveals that coordination diversity of imidazole and phenylacetic acid toward Cu(II) is dependent on pH.



## 2. Experimental

### 2.1. *Materials and physical methods*

All chemicals were commercially available from Sinopharm Chemical Reagent Beijing Co., Ltd. products and used without purification. Powder X-ray diffraction (PXRD) measurements were carried out with a Bruker D8 Focus X-ray diffractometer to check the phase purity. Single crystal X-ray diffraction data were collected with a Rigaku Raxis–Rapid X-ray diffractometer. C, H, and N microanalyses were performed with a Perkin Elmer 2400II CHNO/S elemental analyzer. FT–IR spectra were recorded as KBr pellets from 4000 to 400 $cm^{-1}$ on a Shimadzu FTIR–8900 spectrometer. Combined differential thermal analyses (DTA) and thermogravimetric analyses (TGA) were carried out on preweighed samples from room temperature to 850°C at a heating rate of 10°C $min^{-1}$ in nitrogen using a Seiko Exstar 6000 TG/DTA 6300. Temperature-dependent magnetic susceptibilities were determined with a Quantum Design SQUID Model MPMS-7 magnetometer from 2 to 300 K at an applied field of 5 KOe for **1** and 1 KOe for **2**; diamagnetic corrections were estimated from Pascal's constants ($\chi_{dia} = -347.44 \times 10^{-6} cm^3 mol^{-1}$ for **1**; $-335.37 \times 10^{-6} cm^3 mol^{-1}$ for **2**).

### 2.2. *Synthesis of $Cu_2(Him)_4L_4 \cdot 2H_2O$ (1)*

An aqueous solution of imidazole (0.0681 g, 1.00 mmol) in 5.0 mL of $H_2O$ and a solution of 5.0 mL of $H_2O$ and 5.0 mL of EtOH containing phenylacetic acid (0.1631 g, 1.00 mmol) were added to a stirred solution of $CuCl_2 \cdot 2H_2O$ (0.1705 g, 1.00 mmol) in 10.0 mL of $H_2O$. To the mixture, NaOH (1.0 mol $L^{-1}$) was added dropwise to adjust the pH to 6.50. The mixture formed a blue suspension, which was stirred at room temperature for 30 min and filtered. The residual solid was examined by PXRD and IR spectroscopy (figure S1). The blue filtrate (pH = 6.50) was allowed to stand at room temperature with slow evaporation for one month affording blue block crystals (yield = 39.1% based on $CuCl_2 \cdot 2H_2O$). The phase purity of the product was checked by PXRD patterns by comparing with the simulated PXRD based on single crystal data (figure S1). Anal. Calcd for $C_{44}H_{48}Cu_2N_8O_{10}$ (%): C, 54.10; H, 4.92; N, 11.48. Found (%): C, 53.74; H, 4.66; N, 11.60. IR (KBr pellet, $cm^{-1}$): 3442(m), 3144(m), 3065(m), 2961(w), 2868(w), 1585(vs), 1502(w), 1392(s), 1327(w), 1290(w), 1149(w), 1072(m), 1026(w), 761(w), 708(m), 652(w), 616(w), 574(w), 530(w), 463(w).

### 2.3. *Synthesis of $Cu_3(Him)_2(im)_2L_4$ (2)*

The procedure was similar to **1** except the pH was adjusted to 7.50. Blue block-like crystals were grown from the filtrate by evaporation at room temperature for one month (yield = 48.5% based on $CuCl_2 \cdot 2H_2O$). The phase purity of the product was checked by comparing the PXRD patterns relative to the simulated PXRD based on the single crystal data (figure S1). Anal. Calcd for $C_{44}H_{42}Cu_3N_4O_4$ (%): C, 59.96; H, 4.80; N, 5.59. Found (%): C, 59.54; H, 4.67; N, 5.57. IR (KBr pellet, $cm^{-1}$): 3440(m), 3140(m), 3060(m), 2960(w), 2875(w), 2630(w), 1600(m), 1587(s), 1560(vs), 1500(w), 1380(m), 1260(w), 1226(w), 1140(w), 1080(s), 955(w), 773(w), 729(m), 652(m).



### 2.4. *X-ray crystallography*

Suitable single crystals of **1** and **2** were selected under a polarizing microscope and fixed with epoxy cement on respective fine glass fibers, which are then mounted on a Rigaku R-Axis Rapid IP X-ray diffractometer with graphite-monochromated Mo-K$\alpha$ radiation ($\lambda = 0.71073$ Å) for cell determination and subsequent data collection. The reflection intensities in the $\theta$ range 3.00–27.48° were collected at 293 K using the $\omega$ scan technique. The data are corrected for *Lp* and absorption effects. The SHELXS-97 and SHELXL-97 programs are used for the structure resolution and refinement [15]. The structures are solved by using Patterson methods, and all non-hydrogen atoms located in the subsequent difference Fourier syntheses. After several cycles of refinement, all hydrogen atoms associated with carbon are geometrically generated; the rest of the hydrogen atoms are located from successive difference Fourier syntheses. Finally, all non-hydrogen atoms are refined with anisotropic displacement parameters by full-matrix least-squares with hydrogen atoms with isotropic displacement parameters set to 1.2 times the values for the associated heavier atoms. Detailed information about the crystal data and structure determination is summarized in table 1. Selected interatomic distances and angles for **1** and **2** are given in tables 2 and 3.

## 3. Results and discussion

### 3.1. *Syntheses*

Influence of pH for reaction of $CuCl_2 \cdot 2H_2O$, imidazole (Him), and phenylacetic acid (HL) at a molar ratio of 1:1:1 in a mixed solution of water and ethanol at room temperature was investigated. The mixture was stirred and formed a blue precipitate. Blue microcrystals appeared in the filtrate with pH = 3.6. The characterization of PXRD and IR spectroscopy for the microcrystals is phenylacetate copper ($CuL_2$) (figures S2 and S3). When to the above solution was added NaOH (1 mol $L^{-1}$) dropwisely to adjust the pH to 6.5, a blue amorphous precipitate of phenylacetate copper was formed, which was characterized by infrared spectra and PXRD (figure S3). The filtrate is evaporated slowly at room temperature to obtain blue crystals of $Cu_2(Him)_4L_4 \cdot 2H_2O$ (**1**). When the value of pH was 7.5 by the addition of NaOH (1M), blue block-like crystals of $Cu_3(Him)_2(im)_2L_4$ (**2**) were grown from the filtrate by evaporation. The formed precipitate was affirmed as **2** by IR spectra (figure S4).

Table 1. Summary of crystal data, data collection, structure solution, and refinement details for **1** and **2**.

| Compounds | **1** | **2** |
|---|---|---|
| Empirical formula | $C_{44}H_{48}Cu_2N_8O_{10}$ | $C_{44}H_{42}Cu_3N_8O_8$ |
| Formula mass | 976.00 | 1001.48 |
| Crystal system | Triclinic | Monoclinic |
| Space group | $P\bar{1}$ (no. 2) | $P2_1/c$ (no. 14) |
| Description | Blue block | Blue block |
| Crystal size ($mm^3$) | $0.10 \times 0.10 \times 0.10$ | $0.10 \times 0.10 \times 0.10$ |
| Unit cell dimensions (Å, °) | | |
| $a$ | 10.361(2) | 10.109(2) |
| $b$ | 15.341(3) | 11.779(2) |
| $c$ | 16.584(3) | 19.049(4) |
| $\alpha$ | 114.00(3) | |
| $\beta$ | 93.85(3) | 99.02(3) |
| $\gamma$ | 102.69(3) | |
| Volume (Å$^3$), $Z$ | 2312.8(8), 2 | 2240.1(8), 2 |
| Calculated density ($g\,cm^{-3}$) | 1.402 | 1.485 |
| $F(000)$ | 1012 | 1026 |
| Absorption coefficient ($mm^{-1}$) | 0.964 | 1.472 |
| Refinement method | Full-matrix least-squares on $F^2$ | |
| $\theta$ range for data collection (°) | 3.02–27.46 | 3.00–27.40 |
| Reflections collected | 22,370 | 21,401 |
| Independent reflection | 10,361 [$R$(int) = 0.0286] | 5090 [$R$(int) = 0.0446] |
| Data/restraints/parameters | 7067/24/571 | 3503/0/291 |
| Goodness of fit on $F^2$ | 1.095 | 1.056 |
| Final $R$ indices [$I > 2\sigma(I)$][a] | $R_1 = 0.0555$, $wR_2 = 0.1547$ | $R_1 = 0.0356$, $wR_2 = 0.0982$ |
| $R$ indices (all data)[a] | $R_1 = 0.0879$, $wR_2 = 0.1975$ | $R_1 = 0.0573$, $wR_2 = 0.1129$ |
| Extinction coefficients | 0.0000(8) | 0.0000(4) |
| $A$, $B$ values in weighting scheme[b] | 0.1060, 1.5986 | 0.0581, 0.3392 |
| Largest difference peak and hole (e·Å$^{-3}$) | 1.019 and −0.776 | 0.530 and −0.320 |

[a] $R_1 = \Sigma(|F_o| - |F_c|)/\sum|F_o|$, $wR_2 = [\Sigma w(F_o^2 - F_c^2)^2/\Sigma w(F_o^2)^2]^{1/2}$.
[b] $w = [\sigma^2(F_o^2) + (AP)^2 + BP]^{-1}$ with $P = (F_o^2 + 2F_c^2)/3$.

Table 2. Selected bond lengths (Å) and angles (°) for **1**.

| | | | | | |
|---|---|---|---|---|---|
| Cu1–O1 | 1.994(3) | Cu1–N3 | 1.973(4) | Cu2–O7 | 1.956(3) |
| Cu1–O1$^{\#1}$ | 2.553(3) | Cu2–O5 | 1.968(2) | Cu2–N5 | 1.981(4) |
| Cu1–O3 | 1.969(3) | Cu2–O5$^{\#2}$ | 2.572(3) | Cu2–N7 | 1.982(4) |
| Cu1–N1 | 1.988(4) | | | | |
| O1–Cu1–N1 | 92.5(1) | N3–Cu1–O1$^{\#1}$ | 89.8(1) | O7–Cu2–N5 | 89.7(2) |
| O1–Cu1–N3 | 90.4(1) | N1–Cu1–N3 | 175.1(1) | O7–Cu2–N7 | 90.3(2) |
| O1–Cu1–O3 | 175.5(1) | Cu1–O1–Cu1$^{\#1}$ | 102.5(1) | O7–Cu2–O5$^{\#2}$ | 96.4(1) |
| O1–Cu1–O1$^{\#1}$ | 77.5(1) | O5–Cu2–N5 | 89.8(1) | N5–Cu2–O5$^{\#2}$ | 97.1(2) |
| O3–Cu1–N1 | 89.2(2) | O5–Cu2–N7 | 91.1(1) | N7–Cu2–O5$^{\#2}$ | 91.5(1) |
| O3–Cu1–N3 | 88.2(2) | O5–Cu2–O7 | 173.8(1) | N5–Cu2–N7 | 171.3(2) |
| O3–Cu1–O1$^{\#1}$ | 98.2(1) | O5–Cu2–O5$^{\#2}$ | 77.5(1) | Cu2–O5–Cu2$^{\#2}$ | 102.5(1) |
| N1–Cu1–O1$^{\#1}$ | 94.6(1) | | | | |

| D–H···A | d(D–H) | d(H···A) | ∠DHA | d(D···A) |
|---|---|---|---|---|
| Hydrogen bonding contacts | | | | |
| O9–H1···O2 | 0.80 | 2.04 | 2.842(8) | 179 |
| O9–H2···O4 | 0.81 | 2.06 | 2.867(6) | 179 |
| O10–H3···O8 | 0.80 | 1.89 | 2.686(7) | 180 |
| O10–H4···O6 | 0.80 | 1.97 | 2.772(6) | 180 |
| N2–H22···O4$^{\#3}$ | 0.85 | 2.01 | 2.824(6) | 161 |
| N6–H66···O2$^{\#3}$ | 0.85 | 2.03 | 2.823(7) | 155 |
| N8–H88···O10$^{\#2}$ | 0.85 | 2.02 | 2.850(6) | 164 |
| C5–H5A···O6$^{\#1}$ | 0.93 | 1.97 | 2.852(5) | 158 |
| C8–H8A···O3$^{\#1}$ | 0.97 | 2.47 | 3.402(5) | 162 |
| C27–H27A···O8$^{\#2}$ | 0.93 | 2.50 | 3.316(8) | 147 |
| C30–H30B···O7$^{\#3}$ | 0.97 | 2.49 | 3.527(7) | 136 |

Symmetry transformations used to generate equivalent atoms: #1 = $-x+1$, $-y+1$, $-z+1$; #2 = $-x+1$, $-y+1$, $-z+2$; #3 = $-x+2$, $-y+1$, $-z+1$.

Table 3. Selected bond lengths (Å) and angles (°) for **2**.

| | | | | | |
|---|---|---|---|---|---|
| Cu1–O1 | 1.975(2) | Cu1–N2$^{\#3}$ | 1.960(2) | Cu2–N3 | 1.984(2) |
| Cu1–O3 | 2.020(2) | Cu2–O4 | 1.968(2) | Cu2–N3$^{\#2}$ | 1.984(2) |
| Cu1–N1 | 1.962(2) | Cu2–O4$^{\#2}$ | 1.968(2) | | |
| O1–Cu1–O3 | 167.4(1) | O3–Cu1–N2$^{\#3}$ | 89.3(1) | O4–Cu2–N3$^{\#2}$ | 90.5(1) |
| O1–Cu1–N1 | 91.2(1) | N1–Cu1–N2$^{\#3}$ | 171.3(1) | O4$^{\#2}$–Cu2–N3 | 90.5(1) |
| O1–Cu1–N2$^{\#3}$ | 92.2(1) | O4–Cu2–O4$^{\#2}$ | 180.0(1) | O4$^{\#2}$–Cu2–N3$^{\#2}$ | 89.5(1) |
| O3–Cu1–N1 | 89.2(1) | O4–Cu2–N3 | 89.5(1) | N3–Cu2–N3$^{\#2}$ | 180.0(1) |
| D–H···A | | d(D–H) | d(H···A) | ∠DHA | d(D···A) |
| Hydrogen bonding contacts | | | | | |
| N4–H1···O2$^{\#1}$ | | 0.85 | 1.91 | 171 | 2.754 |
| C10–H10A···O3$^{\#4}$ | | 0.93 | 2.54 | 164 | 3.449 |

Symmetry transformations used to generate equivalent atoms: #1 = $-x$, $y+1/2$, $-z+1/2$; #2 = $-x$, $-y$, $-z$; #3 = $-x$, $y-1/2$, $-z+1/2$, #4 = $1+x$, $y$, $z$.



To gain insight into the influence of pH on the formation of **1** and **2**, the pH was increased to 8.5 with NaOH, producing blue precipitate. The resulting colorless filtrate had very low concentration of Cu(II), with the majority of the Cu(II) present in the precipitate. Infrared spectra (figure S2) show the characteristic peak of Him ($\nu \sim 1070\,cm^{-1}$) and HL ($\nu = 1583,\ 1393\,cm^{-1}$), indicating that the precipitate is a new type of phenylacetate imidazolate copper(II) complex different from **1** and **2**.

As to the above analysis, HL donates protons to Him at pH of 3.6 to form the $H_2im^+$. Because of the limited coordination of $H_2im^+$, Cu(II) was only able to coordinate with $L^-$ to form $CuL_2$. Adjusting the pH to 6.5, protons of HL were neutralized allowing the coordination of Him in **1**. Upon increasing the pH to 7.5, not only was all HL neutralized to $L^-$, but parts of Him were deprotonated to form $im^-$, forming **2**. According to this reasoning, enough NaOH was added to neutralize all the HL and Him to obtain a new ternary complex with Cu(II) ions, $im^-$, and $L^-$. Unfortunately, when the pH was 8, amorphous materials were produced that were difficult to identify. The above analysis shows the formation of **1** and **2** depends largely on the pH; the reactions may be summarized as:

$CuCl_2{\cdot}2H_2O + Him + HL$

- pH = 3.60 → $CuL_2$ (1)
- pH = 6.50 → $Cu_2(Him)_4L_4{\cdot}2H_2O$ **1** (2)
- pH = 7.50 → $Cu_3(Him)_2(im)_2L_4$ **2** (3)
- pH = 8.00 → Non-definited $Cu_x(Him)_y(im)_zL_n$ (4)

### 3.2. *Description of the crystal structures*

**3.2.1. $Cu_2(Him)_4L_4{\cdot}2H_2O$ (1).** The asymmetric unit of **1** contains two Cu(II) ions (Cu1 and Cu2), four imidazoles (Him), four phenylacetates ($L^-$) (denoted as L1, L2, L3, and L4 ligands, which contain O1, O3, O5, and O7, respectively) and two lattice water molecules. As illustrated in figure 1, Cu(II) ions are coordinated by two

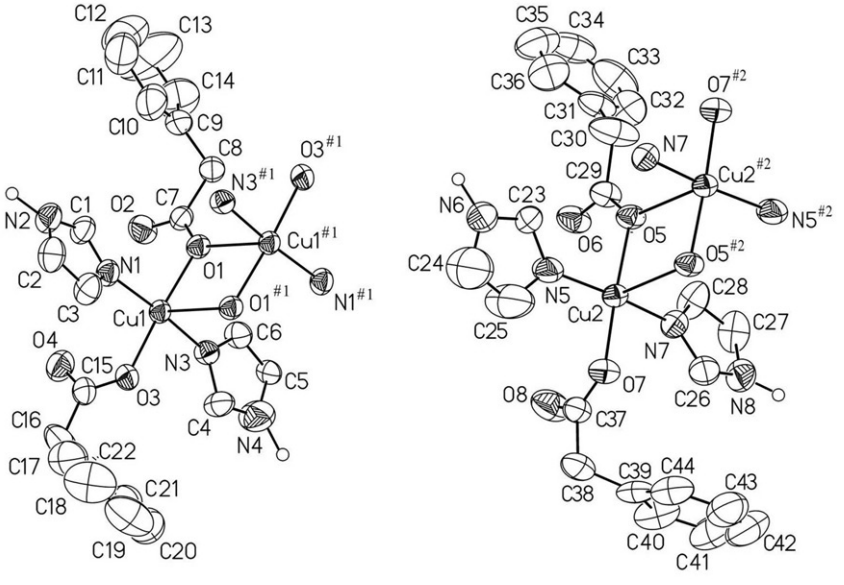


Figure 1. ORTEP view of the Cu(II) dimer along with the atom labeling of **1** with thermal ellipsoids at 45% probability level and all hydrogen atoms except H linking to N were omitted for clarity.

imidazoles and two phenylacetates to form a dinuclear $Cu_2(Him)_4L_4$. Four crystallographically equivalent imidazoles are terminal and both the lengths and angles are normal. Phenylacetates have two different coordination modes. L1 and L3 bridge two Cu with a single oxygen atom, and L2 and L4 are monodentate coordinating with one Cu in syn-mode.

Cu1 displays a $CuN_2O_3$ square-pyramidal geometry. The equatorial plane has two *trans* Him ligands and three carboxylato O atoms of L1 and L2, while the apical position is occupied by a centrosymmetrically related carboxylate $O1^{\#1}$. Cu1 is shifted by 0.0018(5) Å from the equatorial plane toward the apical $O1^{\#1}$. Cu2 has a similar square-pyramidal geometry with the $CuN_2O_3$ chromophore defined by two non-equivalent Him, one O from L4 and two O from two centrosymmetrically related L3 anions. Cu2 is shifted by 0.0224(5) Å from the equatorial plane towards the apical $O5^{\#2}$, which is significantly more than that in Cu1. The axial Cu–O bond lengths are 2.553(3) and 2.572(3) Å and the equator Cu–O/N bond lengths are 1.956(3)–1.994(3) Å and 1.972(4)–1.988(4) Å for Cu1 and Cu2, respectively (table 2). All these bonding parameters are normal [16, 17]. According to the Addison definition, the values of $\tau$ for Cu1 and Cu2 were 0.01 and 0.04, respectively ($\tau = 0$ for an ideal square-pyramid, $\tau = 1$ for an ideal trigonal-bipyramid) [18], indicating that the two square-pyramidal coordination geometries have no significant distortion.

The $CuN_2O_3$ square-pyramids are edged-linked by the single oxygen atoms of L1 or L3 to generate centrosymmetric $Cu_2O_8$ dinuclear complexes. The separation of Cu1···Cu1 and Cu2···Cu2 within the dinuclear units are 3.563(1) and 3.567(1) Å, respectively, similar to the reported {$[Cu(H_2O)_2(C_4H_2O_4)]$ ($C_4H_2O_4$ = fumaric acid)} [19] (3.369(1) Å), $[Cu_2(H_3C–Im)_4(CH_3COO)_4 \cdot 6H_2O]$ [20] (3.4495(4) Å) and {$[Cu_4(mal)_4(bpe)_3]n \cdot 6nH_2O$, mal = malonate dianion; bpe = 1,2-bis(4-pyridyl)ethylene]} [21] (4.949(1), 5.008(1) Å). Lattice water molecules (O9 or O10) donate hydrogen atoms

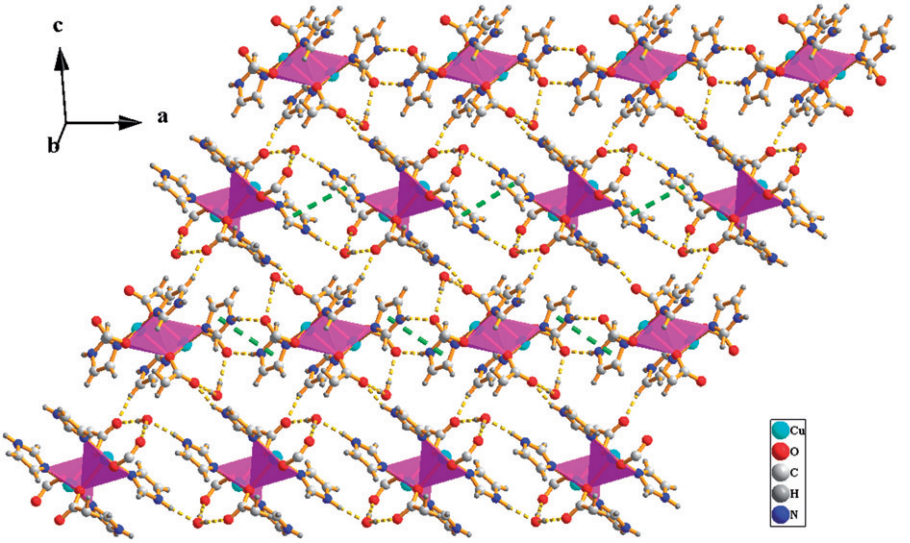


Figure 2. Supramolecular assembly of dinuclear Cu(II) complexes into 2-D layers *via* intermolecular hydrogen bonding and $\pi\cdots\pi$ stacking interactions in **1**; some atoms were omitted for clarity.



to two non-coordinated carboxylics (O2 and O4, or O6 and O8) to form linear O–H···O hydrogen bonds (table 2). The hydrogen-bonding interactions contribute to **1**. The mean interplanar distances between neighboring dinuclear units of the imidazole ring are of 3.40 Å, suggestinga significant intermolecular face-to-face $\pi\cdots\pi$ stacking interactions. Such intermolecular interactions are regarded as the driving forces to assemble dinuclear molecules into 1-D supramolecular chains along the [100] direction, as demonstrated in figure 2. The imidazole donates hydrogen atoms to non-coordinated O of L2 and L4 to form an interlayer hydrogen bond, which is responsible for supramolecular assembly of the 1-D chain into a 2-D supramolecular layer. The 2-D layers are stacked in an ···AAA··· sequence to form the 3-D supramolecular architecture due to van der Waals forces.

**3.2.2. $Cu_3(Him)_2(im)_2L_4$ (2).** The asymmetric unit of 2 contains one and a half Cu (Cu1 and Cu2), one imidazole (Him), one imidazole anion ($im^-$), and two phenylacetates (denoted as L1 and L2, which contain O1 and O3, respectively). Cu1 and Cu2 are centered at the general positions and 2a sites, respectively. As depicted in figure 3, Him and $im^-$ exhibit different coordination behavior. The former is monodentate to Cu(II) and the latter bridges two Cu(II) ions by two nitrogen atoms. The rings of Him and $im^-$ preserve a nearly perfect coplanarity (with the largest distance deviating from the plane by 0.001(1) Å and 0.003(2) Å, respectively). The carboxylate of L1 bonded to one Cu(II) and L2 bridged two Cu's in *anti–syn* fashion.

Cu1 is coordinated by N1 and N2 from two different $im^-$ and two oxygen atoms from L1 and L2 to generate a *trans*-$CuN_2O_2$ plane. Cu2 is coordinated by N from two $im^-$ and two O from two L2 ligands to generate the *trans*-$CuN_2O_2$ plane. Around the Cu1 and Cu2, the largest distance deviating from the ideal plane is −0.182(1) Å and

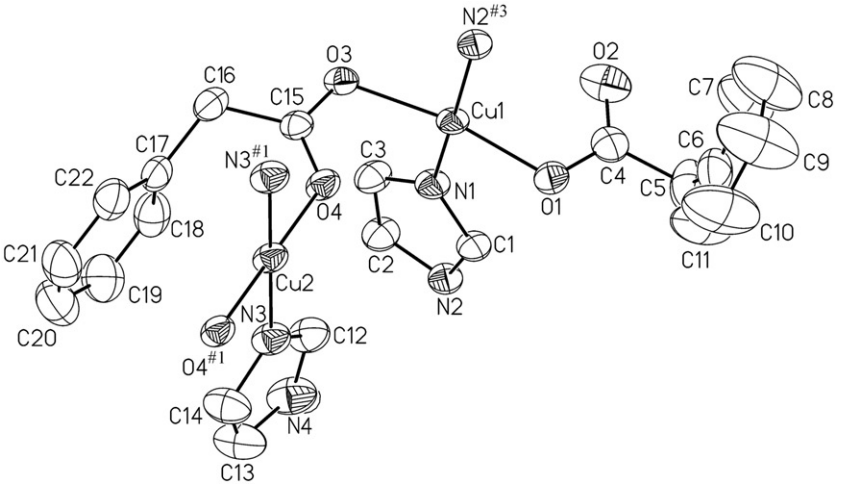


Figure 3. ORTEP view along with the atom labeling of **2** with thermal ellipsoids drawn at 45% probability level and all hydrogen atoms except H linking to N were deleted.

−0.230(2) Å, respectively, indicating that the *trans*-$CuN_2O_2$ planes are slightly distorted to square-pyramidal geometries.

As shown in figure 4, Cu1 and Cu2 are linked by L2 anions in a *syn–anti* mode to form a linear trinuclear $[Cu_3(COO)_2]$, and the Cu1···Cu2 distance is 4.572(1) Å, similar to previous reports. The linear trinuclear $[Cu_3(COO)_2]$ are bridged by $im^-$ to build up a 2D brick–wall layer paralleling (100), and the distance of Cu1···Cu1 is 5.908(1) Å. Nitrogen of Him donates hydrogen bonds to form intra-layer bonds with non-coordinated $O2^{\#1}$ of L1 ($d(N4–H1\cdots O2^{\#1}) = 2.754$ Å, $\angle(N4–H1\cdots O2^{\#1}) = 170.9^\circ$) (table 3). Such hydrogen bonding plays a role in the stability of the 2-D supramolecular layer (figure 5). C10 of phenylacetate donates hydrogen to the carboxylate $O3^{\#4}$ to form hydrogen bonds with $d(C–H\cdots O) = 3.449$ Å and $\angle(C–H\cdots O) = 164^\circ$, leading to a 3D supramolecular architecture (figure 5).

The center Cu(II) in **1** and **2** are coordinated by imidazoles and $L^-$. In **1**, imidazole coordinates monodentate with one Cu(II) as Him. In **2**, imidazole includes the monodentate mode of Him but also is deprotonated to $im^-$ which interlink the trinuclear unit to form the 2D layer. Phenylacetates in **1** have two coordination modes, monodentate and mono-bridging two Cu(II) to form a dinuclear unit. In **2**, one phenylacetate bonds to one Cu(II) and the other phenylacetate coordinates two metals by *syn-anti* fashion to form a linear trinuclear unit.

### 3.3. *Comparison of the relevant copper imidazole complexes*

According to the literature, the most extensively studied complexes for Cu and imidazole could be grouped into three classes with Him, $im^-$ anion, and Him and $im^-$ anion. Generally, Him is terminal, such as the mononuclear compound $Cu(Him)(ClO_4)_2$ [22] and 1-D compound $Cu(tp)(Him)(H_2O)\cdot 2H_2O$ [23]. Him as a free molecule is not common, but found in $Him[Cu(H_2PO_4)_2Cl]\cdot H_2O$ [24]. Typically,

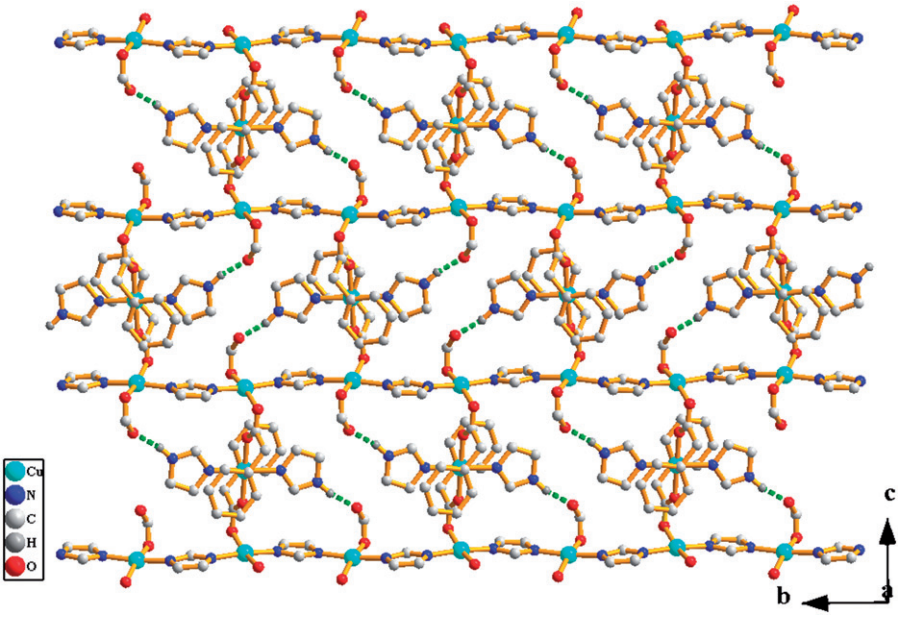


Figure 4. A view of the 2-D layer from the (100) direction of **2**.

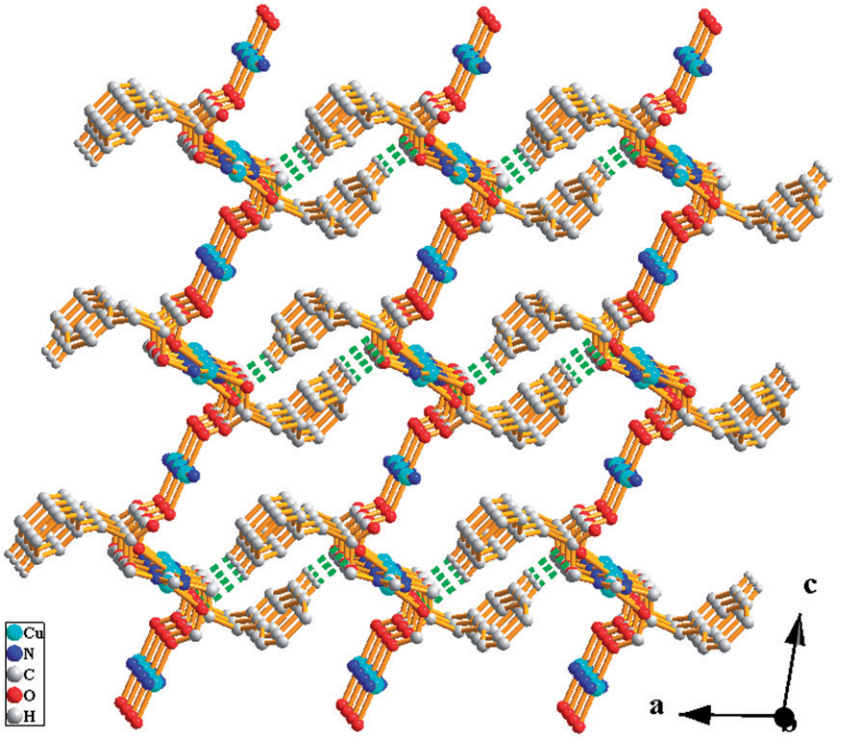


Figure 5. View of packing down the *b* axis. The benzene ring of phenylacetate is omitted for clarity.

$im^-$ bridges two metals by two nitrogen atoms to afford 0-D discrete molecules [25], 1-D zigzag [26], and 2-D layer [12] structures. If Him and $im^-$ were engaged in the same system, Him is terminal and $im^-$ bridges, giving 1-D complexes [14, 23, 27].

### 3.4. *Infrared spectra*

As shown in figure S5, infrared spectra of **1** and **2** exhibit characteristic broad bands centered at 3442 and 3440 $cm^{-1}$, respectively, due to =N–H stretch of Him for **1** and **2** and –OH stretch of lattice water for **1**. The backbone vibration of imidazole has absorptions at 1072 $cm^{-1}$ for **1** and 1080 $cm^{-1}$ for **2**, comparable to those at 1099 $cm^{-1}$ for uncoordinated imidazole. Strong absorptions of the asymmetric stretch of –COO is centered at 1585 $cm^{-1}$ for **1** and 1600 and 1560 $cm^{-1}$ for **2** while the symmetric stretch results in absorptions at 1392 $cm^{-1}$ for **1** and 1380 and 1413 $cm^{-1}$ for **2**. The resulting differences $\Delta\nu_{as-s} = (\nu(CO_2)_{asym} - \nu(CO_2)_{sym})$ are 193 $cm^{-1}$ for **1** and 220 and 147 $cm^{-1}$ for **2**. According to the correlation of $\Delta\nu_{as-s}$ with coordination modes of carboxylates, **1** has monodentate coordination and **2** has mono- and bidentate, consistent with the single-crystal structure determination.

### 3.5. *Thermal analysis*

As shown in figure S6, the TG curve of **1** shows decomposition in three steps; the DTA curve shows three endothermic peaks at 93°C, 108°C, and 231°C. The first weight loss at 40–120°C corresponds to the removal of two lattice water molecules (Calcd 3.69%). The formed anhydrous intermediate "$Cu_2(Him)_4L_4$" is stable on further heating to 144°C. An abrupt weight loss at 144–450°C indicated the decomposition of benzenecarboxylate and complete loss of imidazole with a calculated weight loss of 78.57%; the remaining 17.67% at 450°C is close to the value of 17.62% calculated for 2 mol "CuO" and 1 mol "C." Then there is a slow loss of weight from 450°C to 850°C. The final red residue of 12.40% was identified as Cu (Calcd 13.02%). The TG curve of **2** displays similar thermal behavior to **1** and the DTA curve exhibits an endothermic peak at 172°C. Complex **2** is stable to 160°C and then underwent two successive weight losses. The first of 72.89% from 160°C to 450°C can be assigned to the decomposition of benzenecarboxylate and the complete loss of imidazole with the remaining 27.11% at 450°C, close to the value of 27.42% calculated for 3 mol "CuO" and 3 mol "C." Then slow weight loss of 7.30% from 450°C to 850°C with a red residue of 19.81%, assumed to be Cu, is in agreement with the calculated value of 19.04%.

### 3.6. *Magnetic properties*

Temperature-dependent magnetic susceptibility measurements for **1** and **2** were performed on polycrystalline samples from 2 to 300 K in fixed magnetic fields of 5 kOe and 1 kOe separately, and the magnetic behavior in the form of $\chi_M$ and $\chi_M T$ *versus* $T$ plots are depicted in figure 6 ($\chi_M$ being the magnetic susceptibility per $Cu_2^{4+}$ and $Cu_3^{6+}$ for **1** and **2**, respectively).

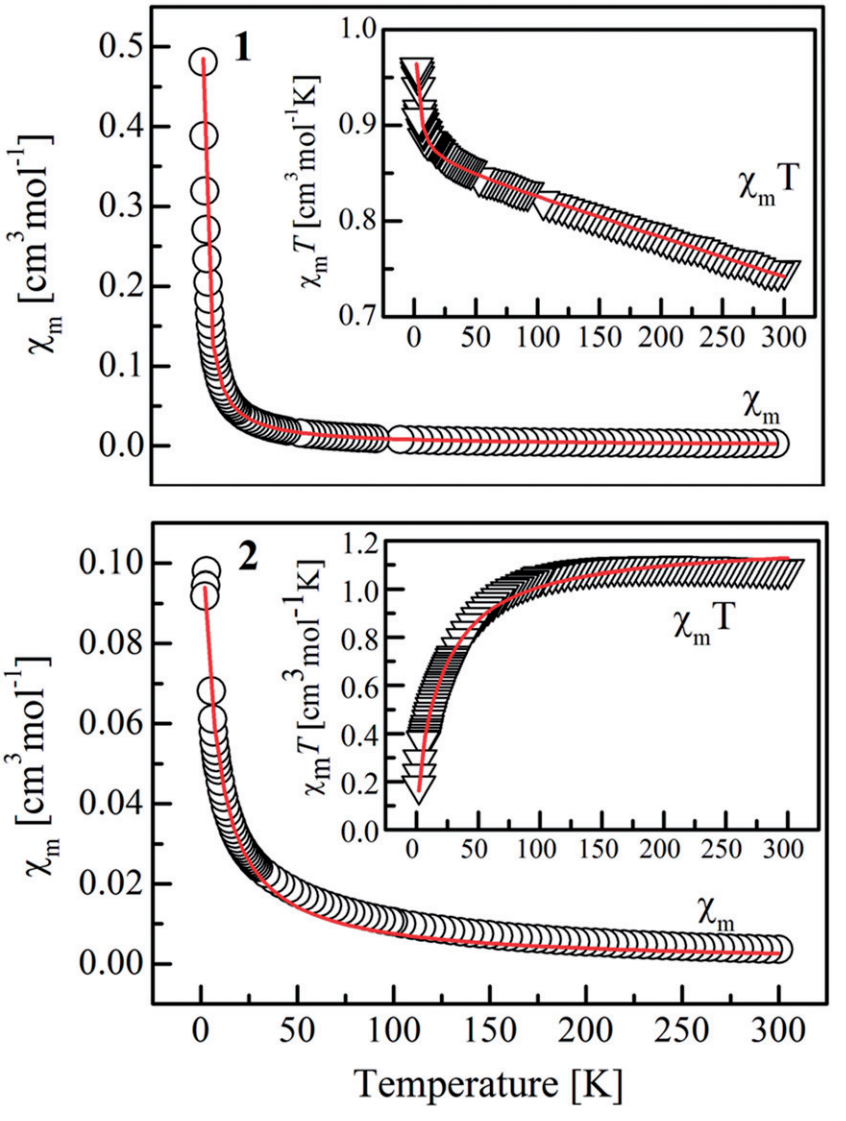


Figure 6. Temperature dependence of the magnetic susceptibilities of **1** and **2** ($\chi_M$ being the magnetic susceptibility per $Cu_2^{4+}$ for **1** and per $Cu_3^{6+}$ for **2**). Solid lines represent the best fits.

For **1**, $\chi_M T$ at room temperature is 0.748 $cm^3\,K\,mol^{-1}$, which exactly corresponds to the spin-only value of 0.748 $cm^3\,K\,mol^{-1}$ expected for two isolated Cu(II) ($S = 1/2$, $g = 2.0$). Upon cooling, $\chi_M T$ gradually increases to 0.902 $cm^3\,K\,mol^{-1}$ at 6.5 K, after which $\chi_M T$ value rises rapidly to the maximum of 0.960 $cm^3\,K\,mol^{-1}$ at 2 K, suggesting overall ferromagnetic interactions between Cu(II) ions (figure 6). The $\chi_M$ can be fit to the Curie–Weiss equation $\chi_M = C/(T-\Theta)$ with the Curie constant $C = 0.875(2)\,cm^3\,mol^{-1}$ and the Weiss constant $\Theta = 0.192(7)$ K, indicating weak ferromagnetic interactions between Cu(II) ions. According to the crystal structure of

**1**, the magnetic structure can be modeled to a dinuclear copper(II), which is bridged by carboxyl. Owing to very weak magnetic interactions between ions, the expression of dinuclear model is corrected using the molecular field approximation, to which the present measured magnetic susceptibility data are fitted [28],

$$\chi_{\mathrm{di}} = \frac{2N\beta^2 g^2}{kT} \times \frac{e^{2J/kT}}{1+3e^{2J/kT}} + Na$$

$$\chi_{\mathrm{M}} T = \frac{\chi_{\mathrm{di}} T}{1-(2zJ'/Ng^2\beta^2)\chi_{\mathrm{di}}}$$

where $J$ represents the coupling constant in binuclear copper(II) units, $zJ'$ is the total exchange parameter between binuclear copper(II) units, $Na$ is the temperature-independent paramagnetic correction factor, and the rest of the parameters have their usual meanings. The best fit is obtained with the values of $g = 2.146(2)$, $J = 0.58(4)\,\mathrm{cm}^{-1}$, $zJ' = -0.10(2)\,\mathrm{cm}^{-1}$, and $R = 1 \times 10^{-5}$ ($R = \Sigma\,(\chi_{\mathrm{obsd}} - \chi_{\mathrm{calcd}})^2/\Sigma\chi^2_{\mathrm{obsd}}$). The fitting results indicate that weak ferromagnetic interactions exist between two Cu(II) ions bridged by carboxyl oxygen, and the value of $J = 0.58\,(4)\,\mathrm{cm}^{-1}$ is similar to the reported value of $0.63\,\mathrm{cm}^{-1}$ in complexes bridged by carboxylate [29].

For **2**, $\chi_{\mathrm{M}}T$ at room temperature is $1.082\,\mathrm{cm}^3\,\mathrm{K\,mol}^{-1}$, slightly lower than the spin-only value of $1.123\,\mathrm{cm}^3\,\mathrm{K\,mol}^{-1}$ expected for three isolated Cu(II) ($S = 1/2$, $g = 2.0$). When the temperature is lowered, $\chi_{\mathrm{M}}T$ slightly increases to a maximum of $1.095\,\mathrm{cm}^3\,\mathrm{K\,mol}^{-1}$ at 210 K, after which $\chi_{\mathrm{M}}T$ value decreases rapidly to $0.964\,\mathrm{cm}^3\,\mathrm{K\,mol}^{-1}$ at 65 K, and then $\chi_{\mathrm{M}}T$ value falls rapidly to $0.183\,\mathrm{cm}^3\,\mathrm{K\,mol}^{-1}$ at 2 K, indicating an overall antiferromagnetic coupling between Cu(II) ions. The $\chi_{\mathrm{M}}$ can be fit to the Curie–Weiss equation $\chi_{\mathrm{M}} = C/(T-\Theta)$ with the Curie constant $C = 0.82(2)\,\mathrm{cm}^3\,\mathrm{mol}^{-1}$ and the Weiss constant $\Theta = -6.8(3)$ K, indicating weak antiferromagnetic interactions between Cu(II) ions.

The Cu(II)'s are interlinked by *syn–anti* $-\mathrm{COO}^-$ of phenylacetate ($J_1$ Cu1–Cu2) and bridging $\mathrm{im}^-$ ($J_2$ Cu1–Cu1) to generate a 2-D layer. Therefore, the magnetic behavior of **2** could be magnetically modeled to a 2-D network, and the two magnetic interactions of $J_1$ and $J_2$ can be described as scheme 1. Regretfully, estimation of the interactions between metals could not be made. By tracing the magnetic exchange literature for Cu(II) with the bridging imidazole anion and carboxylate, the coupling constant of Cu(II) ions with bridging by imidazole range from 0 to $-82\,\mathrm{cm}^{-1}$ [30], and the value by the *syn–anti* bridging mode of carboxyl is 0–10 $\mathrm{cm}^{-1}$ [31]. Hence, the magnetic behavior of **2** will be discussed in two approaches as follows.

(a) Ignoring the magnetic exchange interaction $J_2$ between the imidazole anion interlinked Cu, the two-dimensional magnetic model can be regarded as a trinuclear copper group bridged by *syn–anti* $-\mathrm{COO}^-$. Taking account of the molecular field interactions, the expression to which the $\chi_{\mathrm{M}}T$ of **2** was fitted,

$$\chi_{\mathrm{tri}} = \frac{Ng^2\beta^2}{4kT} \times \frac{10e^{J_1/kT} + e^{-2J_1/kT} + 1}{2e^{J_1/kT} + e^{-2J_1/kT} + 1} + Na$$

$$\chi_{\mathrm{M}} T = \frac{\chi_{\mathrm{tri}} T}{1-(2zJ'/Ng^2\beta^2)\chi_{\mathrm{tri}}}$$

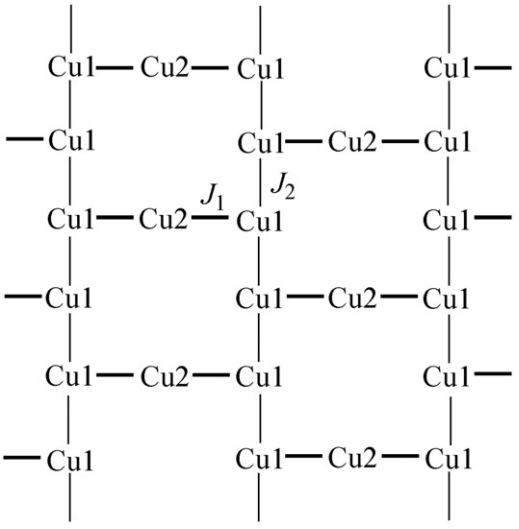


Scheme 1. The magnetic exchange of **2**.

where *Na* is the temperature-independent paramagnetic correction factor, $zJ'$ is the coupling of Cu(II) ions bridged by an imidazole anion, and the rest of the parameters have their usual meanings. The best fit is obtained with the values of $g = 2.09(2)$, $J_1 = -10.24(32)\,\mathrm{cm}^{-1}$, $zJ' = -0.55(7)\,\mathrm{cm}^{-1}$, and $R$ is $6.6 \times 10^{-4}$ ($R = \Sigma (\chi_{\mathrm{obsd}} - \chi_{\mathrm{calcd}})^2/\Sigma\chi^2_{\mathrm{obsd}}$) (figure 5).

(b) Neglecting the magnetic exchange interaction $J_1$ between the *syn–anti* –$COO^-$-bridged Cu1 and Cu2, the 2-D magnetic model can be regarded as 1-D polymeric bands in which copper(II) ions are bridged by an imidazole anion and a mononuclear copper atom. Owing to very weak magnetic interactions between ions, the expression is corrected using the molecular field approximation, to which the present measured magnetic susceptibility data are fitted as follows:

$$\chi'_{\mathrm{M}} = \chi_{\mathrm{chain}} + 2\chi_{\mathrm{mono}}$$

$$\chi'_{\mathrm{M}} = \frac{Ng^2\beta^2}{kT} \times \frac{0.25 + 0.074975x + 0.075235x^2}{1.0 + 0.9931x + 0.172135x^2 + 0.757825x^3} + \frac{2Ng^2\beta^2}{4kT}$$

$$\chi_{\mathrm{M}}T = \frac{\chi'_{\mathrm{M}}T}{1 - (2zJ'/Ng^2\beta^2)\chi'_{\mathrm{M}}}$$

where $x = |J|/kT$, $zJ'$ is the total exchange parameter between copper(II) units and the rest of the parameters have their usual meanings. The best fit is obtained with the values of $g = 2.068(14)$, $J = 28.00(27)\,\mathrm{cm}^{-1}$, $zJ' = -5.46(18)\,\mathrm{cm}^{-1}$, and $R = 6.9 \times 10^{-4}$ ($R = \Sigma (\chi_{\mathrm{obsd}} - \chi_{\mathrm{calcd}})^2/\Sigma\chi^2_{\mathrm{obsd}}$), in which the positive $J$ indicates the ferromagnetic coupling between adjacent copper(II) ions, inconsistent with the magnetic behaviors illustrated by $\chi_{\mathrm{M}}T$ *versus* $T$ plot. Clearly, according to the above analysis, the first approach is more effective in interpreting the magnetic behaviors of **2**.

## 4. Conclusion

Two new complexes, $Cu_2(Him)_4L_4 \cdot 2H_2O$ (**1**) and $Cu_3(Him)_2(im)_2L_4$ (**2**), were synthesized at different pH values. Compound **1** features a dinuclear unit by a caroxylate bridge. In **2**, Cu(II) are bridged by $im^-$ and phenylacetate with the *syn–anti* mode to form a 2-D layer. The structure determinations reveal that the coordination of imidazole and phenylacetate toward copper(II) are dependent upon the pH in the reaction system.



## Supplementary material

Crystallographic data for **1** and **2** are deposited with the Cambridge Crystallographic Data Center, CCDC-862397 (**1**) and -862398 (**2**) [CCDC, 12 Union Road, Cambridge CB2 1EZ, United Kingdom; Fax: (44)1223-336-033; E-mail: deposit@ccdc.cam.ac.uk; website: http://www.ccdc.cam.ac.uk].

## Acknowledgments

This project was supported by the Scientific Research Fund of Ningbo University (Grant No. XKL11058 and XYL11005). Honest thanks are also extended to K.C. Wong Magna Fund from the Ningbo University.

## References

[1] J.P. Zhang, X.C. Huang, X.M. Chen. *Chem. Soc. Rev.*, **38**, 2385 (2009).
[2] M.J. Zaworotko. *Cryst. Growth Des.*, **7**, 4 (2007).
[3] N.C. Gianneschi, M.S. Masar III, C.A. Mirkin. *Acc. Chem. Res.*, **38**, 825 (2005).
[4] L. Kovbasyuk, R. Kramer. *Chem. Rev.*, **104**, 3161 (2004).
[5] L. Brunsveld, B.J.B. Folmer, E.W. Meijer, R.P. Sijbesma. *Chem. Rev.*, **101**, 4071 (2001).
[6] M.C.T. Fyfe, J.F. Stoddart. *Acc. Chem. Res.*, **30**, 393 (1997).
[7] D.L. Caulder, R.N. Raymond. *Acc. Chem. Res.*, **32**, 975 (1999).
[8] W. Neish. *Esperientia (Basel)*, **27**, 860 (1971).
[9] J.Y. Le, X.H. Zhou, K.B. Xing. *Chin. J. Chem.*, **4**, 194 (2000).
[10] X.Y. Le, G. Yang, Q.M. Lu. *Chin. J. Inorg. Chem.*, **18**, 427 (2002).
[11] M. Norberto, B. Silvia, C. Elena, C. Franco, G. Simona, N. Sironi. *Inorg. Chem.*, **40**, 5897 (2001).
[12] X.C. Huang, J.P. Zhang, Y.Y. Lin, X.L. Yu, X.M. Chen. *Chem. Commun.*, 1100 (2004).
[13] R. Boča, M. Hvastijová, J. Kožíšek, M. Valko, H. Ehrenberg, H. Fuess, W. Haase, I. Svoboda, R. Werner. *Inorg. Chem. Commun.*, **8**, 548 (2005).
[14] S.H. Rahaman, H. Chowdhury, D. Bose, G. Mostafa, H.K. Fun, B.K. Ghosh. *Inorg. Chem. Commun.*, **8**, 1041 (2005).
[15] G.M. Sheldrick. *SHELXS-97*, *Program for Crystal Stucture Refinement*, *and SHELXL-97*, *Program for Crystal Stucture Solution*, Göttingen University, Germany (1997).
[16] I. Gun. *Acta Chem. Scand.*, **27**, 3523 (1973).
[17] J. Server-Carrió, E. Escrivà, J. Folgado. *Transition Met. Chem.*, **21**, 541 (1996).
[18] A.W. Addison, N. Rao. *J. Chem. Soc., Dalton Trans.*, 1349 (1984).
[19] Y.Q. Zheng, H.Z. Xie. *J. Coord. Chem.*, **58**, 539 (2005).
[20] Y. Boukari, A. Busnot, F. Busnot, A. Leclaire, M.A. Bernard. *Acta Crystallogr., Sect. B*, **38**, 2458 (1982).
[21] F.S. Delgado, J. Sanchiz, C. Ruiz-Peŕez, F. Lloret, M. Julve. *Inorg. Chem.*, **42**, 5938 (2003).

[22] J. Wang, X. Liu, Y. Sun, L. Yan, S. He. *J. Coord. Chem.*, **64**, 1554 (2011).
[23] T.C. Stamatatos, S.P. Perlepes, C.P. Raptopoulou, A. Terzis, C.S. Patrickios, A.J. Tasiopoulos, A.K. Boudalis. *Dalton Trans.*, 3354 (2009).
[24] S. Neeraj, T. Loiseau, C.N.R. Rao, A.K. Cheetham. *Solid State Sci.*, **6**, 1169 (2004).
[25] W. Plass, A. Pohlmann, P.S. Subramanian, D. Srinivas. *Z. Anorg. Allg. Chem.*, **628**, 1377 (2002).
[26] N. Koyama, R. Watanabe, T. Ishida, T. Nogami, T. Kogane. *Polyhedron*, **28**, 2001 (2009).
[27] K. Sakai, T. Akutagawa, T. Nakamura. *Eur. J. Inorg. Chem.*, 116 (2011).
[28] C. Ruiz-Pérez, J. Sanchiz, M.H. Molina, F. Lloret, M. Julve. *Inorg. Chem.*, **39**, 1363 (2000).
[29] Y. Journaux, J. Sleten, O. Kahn. *Inorg. Chem.*, **24**, 4063 (1985).
[30] R. Baggio, M.T. Garland, J. Manzur, O. Peña, M. Perec, E. Spodine, A. Vega. *Inorg. Chim. Acta*, **286**, 74 (1999).
[31] X.M. Zhuang, T.B. Lu, S. Chen. *Inorg. Chim. Acta*, **358**, 2129 (2005).